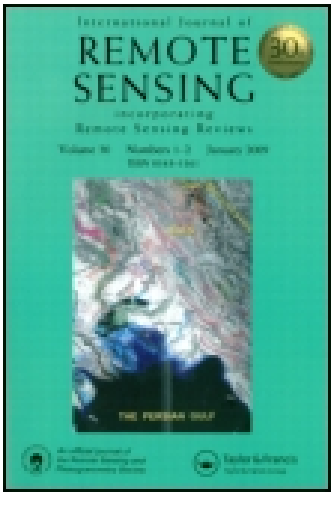

International Journal of Remote Sensing

Publication details, including instructions for authors and subscription information:
http://www.tandfonline.com/loi/tres20

Satellite and ground-based monitoring of smoke in the atmosphere during the summer wildfires in European Russia in 2010 and Siberia in 2012

G.I. Gorchakov[a], S.A. Sitnov[a], M.A. Sviridenkov[a], E.G. Semoutnikova[b], A.S. Emilenko[a], A.A. Isakov[a], V.M. Kopeikin[a], A.V. Karpov[a], I.A. Gorchakova[a], K.S. Verichev[a], G.A. Kurbatov[b] & T.Ya. Ponomareva[c]

[a] A.M. Obukhov Institute of Atmospheric Physics, Russian Academy of Sciences, Moscow, Russia

[b] Faculty of Physics, M.V. Lomonosov Moscow State University, Moscow, Russia

[c] Federal Service for Hydrometeorology and Environmental Monitoring, Hydrometeorological Centre of Russia, Moscow, Russia

Published online: 28 Aug 2014.

To cite this article: G.I. Gorchakov, S.A. Sitnov, M.A. Sviridenkov, E.G. Semoutnikova, A.S. Emilenko, A.A. Isakov, V.M. Kopeikin, A.V. Karpov, I.A. Gorchakova, K.S. Verichev, G.A. Kurbatov & T.Ya. Ponomareva (2014) Satellite and ground-based monitoring of smoke in the atmosphere during the summer wildfires in European Russia in 2010 and Siberia in 2012, International Journal of Remote Sensing, 35:15, 5698-5721

To link to this article: http://dx.doi.org/10.1080/01431161.2014.945008

International Journal of Remote Sensing, 2014
Vol. 35, No. 15, 5698–5721, http://dx.doi.org/10.1080/01431161.2014.945008

Taylor & Francis
Taylor & Francis Group

Satellite and ground-based monitoring of smoke in the atmosphere during the summer wildfires in European Russia in 2010 and Siberia in 2012

G.I. Gorchakov[a], S.A. Sitnov[a]*, M.A. Sviridenkov[a], E.G. Semoutnikova[b], A.S. Emilenko[a], A.A. Isakov[a], V.M. Kopeikin[a], A.V. Karpov[a], I.A. Gorchakova[a], K.S. Verichev[a], G.A. Kurbatov[b], and T.Ya. Ponomareva[c]

[a]*A.M. Obukhov Institute of Atmospheric Physics, Russian Academy of Sciences, Moscow, Russia;* [b]*Faculty of Physics, M.V. Lomonosov Moscow State University, Moscow, Russia;* [c]*Federal Service for Hydrometeorology and Environmental Monitoring, Hydrometeorological Centre of Russia, Moscow, Russia*

(*Received 25 July 2013; accepted 22 June 2014*)

Using Moderate Resolution Imaging Spectroradiometer (MODIS) (Aqua and Terra satellites) and *in situ* observations, a comparative analysis of two large-scale smoke events caused by the summer wildfires in European Russia (ER) in 2010 and Western Siberia (WS) in 2012 was carried out. In the 5-day periods of the extreme smoke pollution (5–9 August 2010 in ER and 27–31 July 2012 in WS), the number of active fires in the equal territories, confined by the coordinates 47°–65° N, 25°–55° E and 51°–70° N, 71°–104° E, was found to be 4754 for ER and 3823 for WS. With this, the regional mean aerosol optical depths (AODs) were found to be (1.02 ± 0.02) and (1.00 ± 0.04), not much differing for both the events. The regional mean aerosol radiative forcing effects at the top (R_1) and the bottom (R_2) of the atmosphere over ER/WS according to MODIS observations were estimated to be (−61 ± 1) and (−54 ± 2) W m^{-2}, and (−107 ± 2) and (−96 ± 3) W m^{-2}, respectively. At the same time, the local values of AOD and the local absolute values of R_1 and R_2 over WS were considerably higher than those over ER. MODIS AOD (L3) data during the wildfires of 2010 were validated by AOD data obtained by the sun-sky photometer CIMEL, operating at the AERONET station Zvenigorod. The rates of radiative heating of the smoky atmosphere over ER and WS were also estimated and compared with the existed temperature anomalies, obtained using National Centers for Environmental Prediction National Center for Atmospheric Research reanalysis data. Optical and microphysical properties of smoke aerosols during the wildfires in ER and WS also revealed some similar characteristics. The aerosols were mostly found in the submicron-size fraction and characterized by very high single-scattering albedos (0.95–0.98). In the dense smoke conditions, the degree of linear polarization at the scattering angle 90° during both the events decreased to negative values ranging between −0.1 and −0.15. The optical properties of smoke aerosols were mainly conditioned by unusually narrow particle size distribution.

1. Introduction

Summer wildfires in Russia are often associated with heat waves and droughts, caused by the phenomenon of atmospheric blocking (Mokhov 2011). According to model estimates, if global warming continues, one should expect growth in the number of wildfires over the territory of Russia (Mokhov, Chernokulsky, and Shkolnik 2006). Aerospace monitoring is

*Corresponding author. Email: sitnov@ifaran.ru

an effective tool for studying mass wildfires and associates with them large-scale smoke events (Van Donkelaar et al. 2011; Witte et al. 2011; Val Martin et al. 2012). In combination with data from ground-based systems, it provides rather complete information about the climatic and environmental effects of smoke pollution. In the last half century, there were three strong large-scale smoke episodes in European Russia (ER) caused by the wildfires of 1972, 2002, and 2010 (Chubarova et al. 2011). While studying the characteristics of smoke aerosols during the wildfires of 2002 in ER, Gorchakov et al. (2004) retrieved aerosol number particle size distribution for radii from 0.03 to 10 μm, characterized by a median radius 0.05–0.12 μm, and found that the single scattering albedo (SSA) in the visible range varied from 0.95 to 0.98. Gorchakov et al. (2004) also found that the carbon monoxide (CO) concentration reached the value 15 mg m^{-3}, while the concentrations of Zn, Cd, Pb, Ni, Co, and Cr in Moscow exceeded 8–40 times corresponding concentrations in the Moscow region. The optical and microphysical properties of smoke in the surface layer and atmospheric column during the summer wildfires of 2010 in ER were documented by Gorchakov, Sviridenkov, et al. (2011). The changes in surface gas composition and in mass concentration of PM10 in Moscow and the Moscow region in the summer of 2010 have been studied by Golitsyn et al. (2011) and Gorchakov, Semoutnikova, et al. (2011) using the data from Mosecomonitoring. According to their results, the concentrations of smoke aerosol (PM10) and soot in Moscow reached the values 1.6–1.7 mg m^{-3} and 22 μg m^{-3}, while the concentration and total content of CO achieved the values 37.5 mg m^{-3} and 6 g m^{-2} (1.27×10^{18} mol cm^{-2}), respectively. Spatio-temporal evolution of smoke pollution over ER during the summer wildfires of 2010 was also intensively studied using satellite data (Sitnov 2011a, 2011b). It was found that daily gridded (1° × 1°) values of aerosol optical depth (AOD) over ER during this period reached the value 4.86. A joint analysis of satellite and ground-based data allowed Sitnov et al. (2013) to estimate the mass content of smoke aerosol in the atmospheric column and evaluate the regional radiative and thermal effects of smoke during the summer 2010 wildfires.

In this paper, we consider in detail the optical, radiative, and thermal effects of the large-scale smoke events caused by the wildfires in ER in the summer of 2010 and compare them with those caused by the wildfires in Western Siberia (WS) in the summer of 2012. We also compare optical and microphysical properties of smoke during both wildfire events.

2. MODIS instruments and algorithms

The Moderate Resolution Imaging Spectroradiometer (MODIS) is a 36-channel imaging spectrometer measuring the reflected solar radiation and Earth's thermal emission in the wavelength range of 0.4–14.4 μm (Salomonson et al. 1989) with a spatial resolution from 250 to 1000 m, depending on channel. The optical system of the instrument scans a 2330 km-wide swath in a direction perpendicular to the satellite trajectory and this allows MODIS to provide daily global coverage of measurements in the extratropics. The MODIS instruments operate on board the Aqua and Terra satellites, launched respectively on 4 May 2002 and 18 January 1999 in sun-synchronous polar orbits with an altitude of about 700 km, inclination of 98°, and orbital period of 98 min. Daytime MODIS/Terra and MODIS/Aqua observations are made at the descending and ascending orbits with equator crossing times of 10:30 and 13:30, respectively (http://modis.gsfc.nasa.gov).

The MODIS algorithm for retrieving AOD [$\tau(\lambda)$] over the land is based on measuring the intensities (ρ) of the reflected solar radiation at the wavelengths λ = 0.47, 0.66, 1.24,

and 2.13 μm, selecting the proper aerosol models of fine and coarse aerosols, and utilizing look-up tables, based on the solution of the radiative transfer equation for given observational geometry, region, and season (Levy et al. 2007). The retrieval error of AOD over land is estimated to be $\pm 0.05 \pm 0.15\ \tau$ (Kaufman et al. 1997).

The algorithm for detecting active fires uses the contextual analysis of brightness temperatures in the 4 μm (T_4) and 11 μm (T_{11}) channels in the ground pixels of 1 km × 1 km in size (Giglio et al. 2003). The confidence of the active fire detection is quantified by three (low, nominal, and high) confidence levels. This paper uses the data characterized by a high confidence level ($80 \le P \le 100\%$). The fire radiative power (FRP) is calculated using the empirical formula: $\mathrm{FRP}\ [MW] = 4.34 \times 10^{-19}\ ((T_4)^8 - (\overline{T_4})^8)\, S$, where T_4 and $\overline{T}_4$ are the 4 μm brightness temperatures of a fire-containing pixel and its neighbourhood, respectively; and S is the pixel area, which takes into account the areal distortion, in km^2 (Justice et al. 2002).

3. Data used

AOD observations at the wavelength of 0.55 μm ($\tau_{0.55}$) from MODIS instruments (both Aqua and Terra platforms) were used. MODIS products MOD08_D3/MYD08_D3 containing coll. 5.1, L3 AOD data were obtained through the LAADS Web server (http://ladsweb.nascom.nasa.gov). L3 products are the initial (L2) retrievals, daily averaged within the grid cells 1° × 1° (Hubanks et al. 2008). At the latitude of Moscow (55.75°), the grid cell 1° × 1° corresponds to 111 km × 63 km (latitude × longitude). The MODIS cloud mask cloud fraction data were taken from the Giovanni interactive visualization and analysis system (http://disc.sci.gsfc.nasa.gov/giovanni), developed and serviced by NASA GES DISC (Acker and Leptoukh 2007). MODIS active fire data products MOD14/MYD14 (L2, V2.4) were obtained through the Fire Information for Resource Management System (http://firefly.geog.umd.edu), developed and maintained by the University of Maryland (USA) with the support of NASA (Davies et al. 2009).

For validation of MODIS AOD measurements, ground-based AOD observations from the sun-sky photometer CIMEL CE-318 operated at the AERONET station Zvenigorod (Holben et al. 1998) were used. The station is located on the territory of the Zvenigorod Scientific Station (ZSS) of the A.M. Obukhov Institute of Atmospheric Physics. Corresponding AOD L1.5 data are available at: http://aeronet.gsfc.nasa.gov.

700 hPa wind was used to analyse the influence of atmospheric dynamics on the smoke plume evolution over ER. The wind at this level, better than the winds at the underlying and overlying levels, represents general patterns of atmospheric dynamics in the region. Daily wind fields, presented by stream lines, were calculated using the archives of meteorological fields in the Hydrometeorological Research Centre of Russia with the help of the analysis and visualization system GrADS (http://www.iges.org/grads). The average wind vectors for 1–10 August 2010 were also calculated using the daytime (12 UTC) radiosonde launches at the 25 upper-air stations (Sitnov and Mokhov 2013). Aerological data were taken from the archive of the upper-air observations at the University of Wyoming (http://weather.uwyo/uppeair). The data from National Centers for Environmental Prediction National Center for Atmospheric Research (NCEP/NCAR) reanalysis (Kalnay et al. 1996) were also used. Spatial distributions of the daily mean temperatures over ER at isobaric surfaces of 925, 850, 700, and 500 hPa in 2000–2010 were obtained through the server: http://www.esrl.noaa.gov/psd/data/gridded/data.ncep.reanalysis.html.

Surface PM10 and CO concentrations as well as CO in the boundary layer in Moscow and the Moscow region were obtained from Mosecomonitoring State Environmental Protection Enterprise (http://www.mosecom.ru). The angular scattering coefficients and the degree of linear polarization of the scattered light in the smoky atmosphere in the summer of 2010 were measured with the help of the nephelometer-polarimeter PhAN that operates at ZSS (Sviridenkov et al. 2006).

4. Results and discussion

4.1. Comparison of MODIS L3 AOD data with AERONET AOD data

MODIS AOD observations have been repeatedly validated by AOD observations of the sun/sky photometer CIMEL (AERONET network) in situations of low and moderate aerosol pollution (e.g. Ichoku et al. 2002; Levy et al. 2010; More et al. 2013). The error of CIMEL AOD observations in the visible range does not exceed 0.01 (Holben et al. 1998), and observations of these instruments were often taken as reference. Using AERONET AOD measurements at over 300 sites as ground truth, Levy et al. (2010) found that 68.8% of MODIS-retrieved AOD (L2) values fell within an expected error (EE) bounds of $\pm(0.05 + 0.15\tau)$. Recently, More et al. (2013) showed that 68% to 84% of the MODIS AODs in 2008–2010 over Pune (India) were within the EE. Extreme smoke pollution of the atmosphere over ER due to summer 2010 wildfires has provided a unique opportunity to validate MODIS observations in a very wide range of AOD variations.

Figure 1(*a*) shows the daily AOD ($\tau_{0.55}$) values obtained by MODIS instruments near ZSS (ground pixel 55°–56° N, 36°–37° E) during the period from 15 July to 31 August 2010 and the daily mean AOD values ($\tau_{0.55}$) obtained using observations of the sun-sky photometer CIMEL, operating at the AERONET station Zvenigorod (55.7° N, 36.78° E). Due to additional attenuation detected in the photometer channels, CIMEL observations have been corrected using the criterion of independence (on average) of AOD on the zenith angle of the sun during the period of air mass rapid change at sunrise and sunset (for more details of the data correction, see Chubarova et al. 2012). Figure 1(*a*) shows that during wildfires the ground-based and satellite AOD observations were characterized by a similar temporal evolution, in particular the timings of the CIMEL AOD extrema and the MODIS (Aqua/Terra) AOD extrema during the period from 29 July to 18 August 2010 exactly coincide with each other. Correlation coefficients between AOD MODIS Aqua/Terra and AOD CIMEL as well as corresponding standard deviations in this period were equal to 0.92/0.95 and ±0.17/±0.09, respectively. Obviously, the random discrepancies between satellite and ground-based AOD observations could be largely conditioned by different spatial and temporal averaging of smoke inhomogeneities in 1° × 1° grid MODIS data and local CIMEL measurements.

Along with this, there are noticeable systematic differences between satellite and ground-based data. It can be seen that during the period under review, MODIS instruments overestimate high AOD values and underestimate relatively low AOD values ($\tau_{0.55} < 0.75$) in comparison with CIMEL (Figures 1(*b*) and (*c*)). Overestimation of AODs by MODIS during wildfires could be explained by the fact that smoke aerosols in the summer of 2010 were mostly found in the submicron-size fraction and characterized by very high SSA values in the range 0.95–0.98 (Gorchakov, Sviridenkov, et al. 2011). It is known that under heavy aerosol loading conditions and in fine-dominated cases, MODIS overestimates AOD where the observed SSA is greater than that assumed for retrievals (Levy et al. 2010). Underestimation of AODs by MODIS during the period before the mass fires could be in part due to imperfectness of information about the

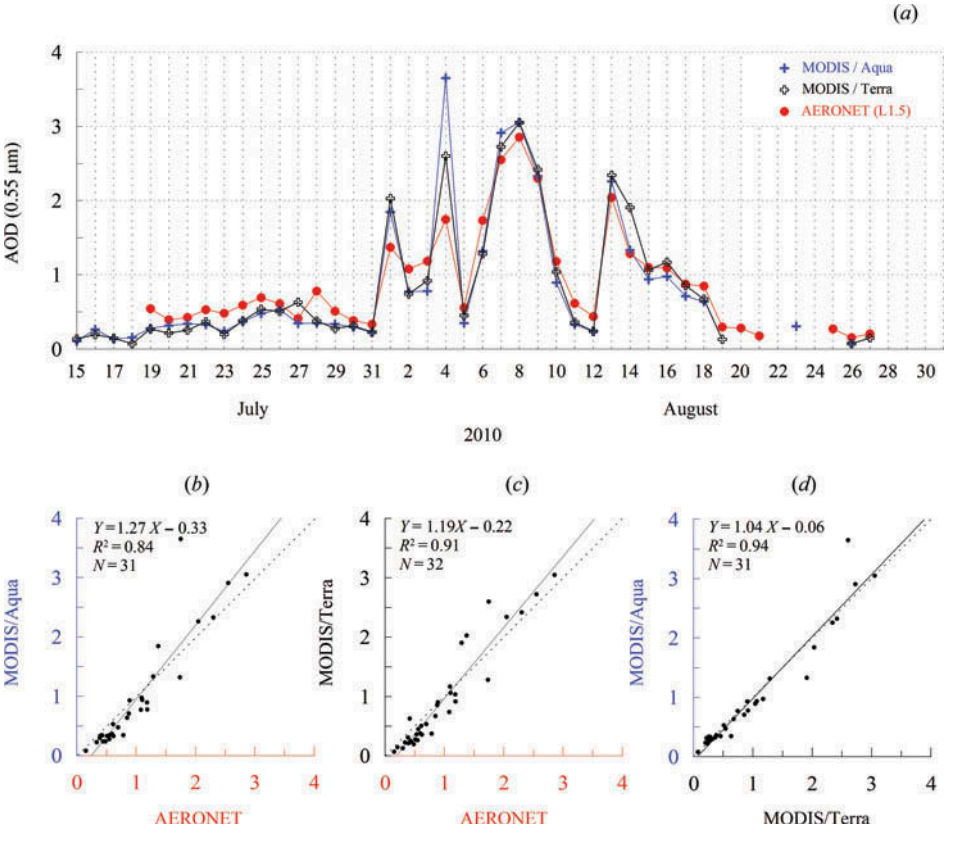

Figure 1. MODIS AOD (L3) data ($\tau_{0.55}$) over the ground pixel 55°–56° N and 36°–37° E and the daily mean AOD data ($\tau_{0.55}$) obtained using the sun-sky photometer CIMEL, operating at the AERONET station Zvenigorod (55.7° N, 36.8° E) during 15 July to 27 August 2010: (*a*) time series; (*b–d*) scatter plots.

regional surface reflectance and aerosol type under the extreme heat wave over ER in July 2010, which are needed for accurate AOD retrievals (Levy et al. 2010; More et al. 2013).

There are also some factors which can lead to underestimation of average AOD values obtained using both the satellite and ground-based observations. During the mass wildfires in the summer of 2010, the local aerosol pollution could exceed the upper limit of the operating range of the MODIS AOD algorithm. In addition, the pixels containing dense smoke could be diagnosed as clouds and, therefore, excluded from the processing (Van Donkelaar et al. 2011). These circumstances tend to lower average AOD values, calculated on the basis of MODIS AOD observations during wildfires (e.g. daily 1° × 1° grid data). On the other hand, the CIMEL automatic procedure of cloud screening is based on analysis of the variability of a series of observations (triplet). In smoky conditions, inhomogeneities of smoke passing through the sun disk could be diagnosed as passing clouds and, as a result, filtered out. The latter circumstance leads to underestimation of the daily mean AOD values obtained on the basis of CIMEL observations. Nevertheless, despite the existing differences, a comparison of satellite and ground-based data reveals satisfactory agreement between MODIS AOD (L3) data and CIMEL AOD local data during the summer 2010 wildfires. Figure 1(*d*) evidences the self-consistency of AODs data from two MODIS instruments.

4.2. Analysis of satellite observations

4.2.1. Smoke events in European Russia in 2010 and in Siberia in 2012

Both episodes of large-scale smoke pollution were caused by wildfires. The quantitative characteristics of fires, cloud cover, AOD, as well as radiative and thermal effects of smoke were compared for the periods 5–9 August 2000 and 27–31 July 2012 over the regions restricted by the coordinates 47°–65° N, 22°–55° E (ER) and 51°–70° N, 71°–104° E (WS). These domains represent territories of the same area (about 4 million km^2), centred on clusters of the most intensive fires. The selected time intervals are the periods of maximum smoke pollution over the territories under consideration. Since large-scale atmospheric dynamics played an important role in the formation and evolution of a smoke plume, spatial distributions of studied characteristics are visualized over the larger territories restricted by the coordinates 40°–70° N, 15°–65° E, encompassing Eastern Europe, and 44°–75° N, 70°–125° E, encompassing the West Siberian Plain and part of the Central Siberian Plateau.

The distributions of active fires over ER during the period 5–9 August 2010 and over WS during the period 27–31 July 2012 are shown in Figures 2(*a*) and (*b*). The total numbers of hotspots over ER and WS during these periods reached the values of 4754 and 3823 with the mean radiative power of a fire equal to 80.2 and 80.5 MW, respectively. Atmospheric circulation over ER in early August 2010 was conditioned by monopole-type blocking, or omega block (Tang et al. 2009), with a high-pressure region centred at 57° N, 42° E (Figure 2(*c*)). The meteorological situation over WS at the end of July 2012 was also conditioned by a blocking anticyclone, but the pattern of atmospheric circulation was more complicated due to dipole-type blocking, or Rex block (Huang et al. 2007) (Figure 2(*d*)). The 700 hPa geopotential height (H700) over ER was significantly higher than H700 over WS, reaching in early August the value of 3260 gpm (cf. Figures 2(*c*) and (*d*)). The descending motions of air associated with the stronger anticyclone over ER led to significant adiabatic heating of air, which contributed to the decrease in cloud cover. As a consequence, the cloud fraction over the territory of ER was half as much compared with that over WS (0.22 and 0.41, respectively; cf. Figures 2(*e*) and (*f*)).

The spatial distribution of AOD over ER during the period 5–9 August 2010 is presented in Figure 3(*a*). The regional mean AOD in this period was equal to 1.02 ± 0.02, while the maximum local AODs (at the resolution of 1° × 1°) reached 3.16. The spatial distribution AOD over WS during the period 27–31 July 2012 is shown in Figure 4(*a*). For this event, the regional mean AOD was found to be approximately the same (1.00 ± 0.04), while the maximum local AODs reached 4.43 (the ground pixel 60°–61° N, 88°–89° E). It is worth noting that according to the ground-based AOD measurements at the AERONET station Tomsk-22 (56.5° N, 84.0° E), the maximum AOD value (at 0.55 μm) in this period exceeded 5.0 (Sakerin et al. 2013).

Figure 5 shows the daily spatial distributions of AOD and the positions of active fires as well as the wind fields (streamlines) during the period of extreme smoke pollution that occurred in the centre of ER from 5 to 9 August 2010. To suppress the small inhomogeneities of the AOD field, the distributions were smoothed by matrix moving average operator 3° × 5° (latitude × longitude), which corresponds to 330 km × 315 km at the latitude of Moscow. The smoothing decreases the local AOD maxima by an average of 28%, but makes more clear common patterns of the distributions.

The clusters of wildfires were detected in the centre of ER, in the south of ER (Northern Black Sea Coast), and in the northeast of the territory (Northern Urals). In the centre, the number of fires was approximately constant in this period, in the south it

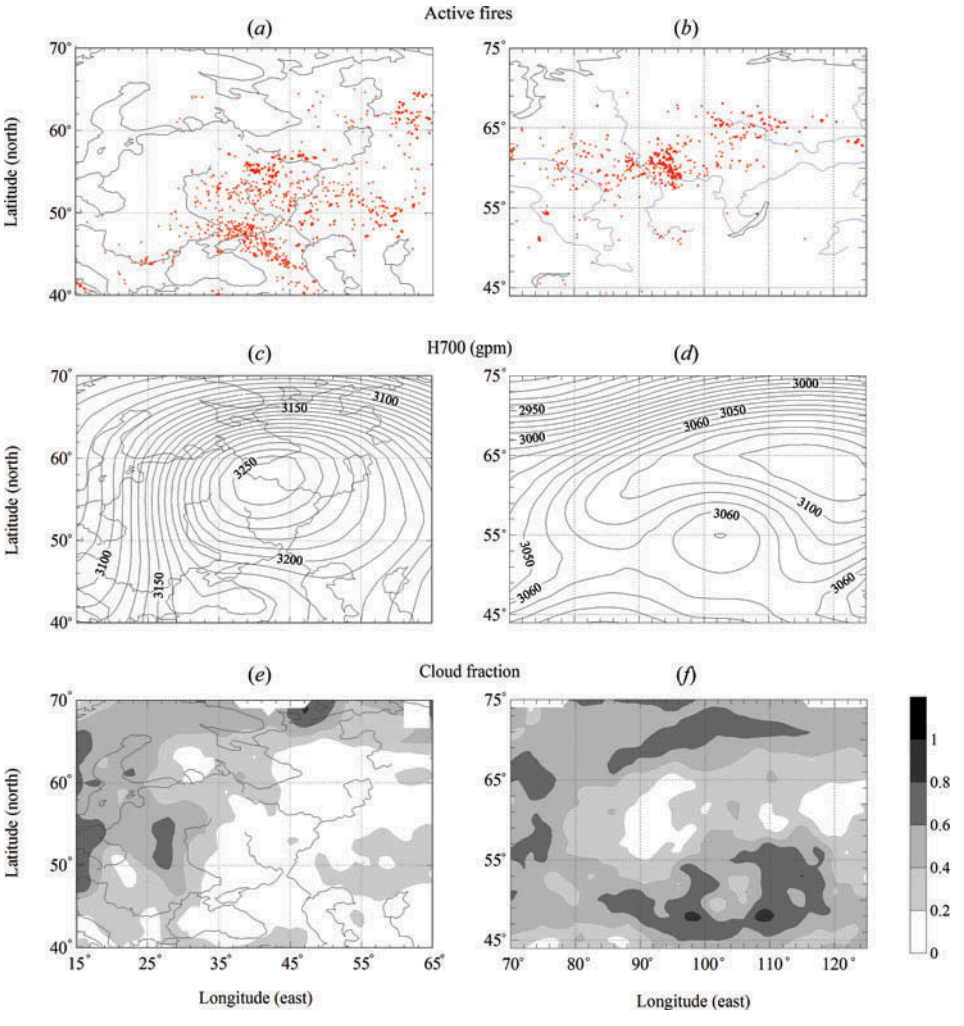

Figure 2. Spatial distributions of active fires (*a, b*), 700 hPa geopotential heights (*c, d*), and cloud fraction (*e, f*) over ER during 5–9 August 2010 (*a, c, e*) and over WS during 27–31 July 2012 (*b, d, f*).

decreased with time, while in the northeast the number of fires increased from 5 until 7 August (Figures 5(*a*)–(c)) and decreased from 7 until 9 August (Figures 5(*c*)–(*e*)), reaching a peak on 7 August.

A comparison of the spatio-temporal evolutions of AOD and active fires in Figure 5 shows that the spatial distribution of smoke over ER has (in a whole) little similarity with the spatial distribution of smoke sources. Also, the temporal variations of regional AOD were not directly related with the changes of burning intensity in the above-mentioned fire clusters. Some exception took place on 6 August when the AOD maximum was centred over the burning area and a spatial distribution of AOD reflected the distribution of fires being oriented in the SW–NE direction. A joint analysis of AOD distributions and wind fields shows that spatio-temporal evolution of AOD during 5–9 August 2010, to a great extent, was conditioned by regional atmospheric circulation caused by blocking anticyclone. Smoke has been involved in the anticyclonic circulation, characterized by weak

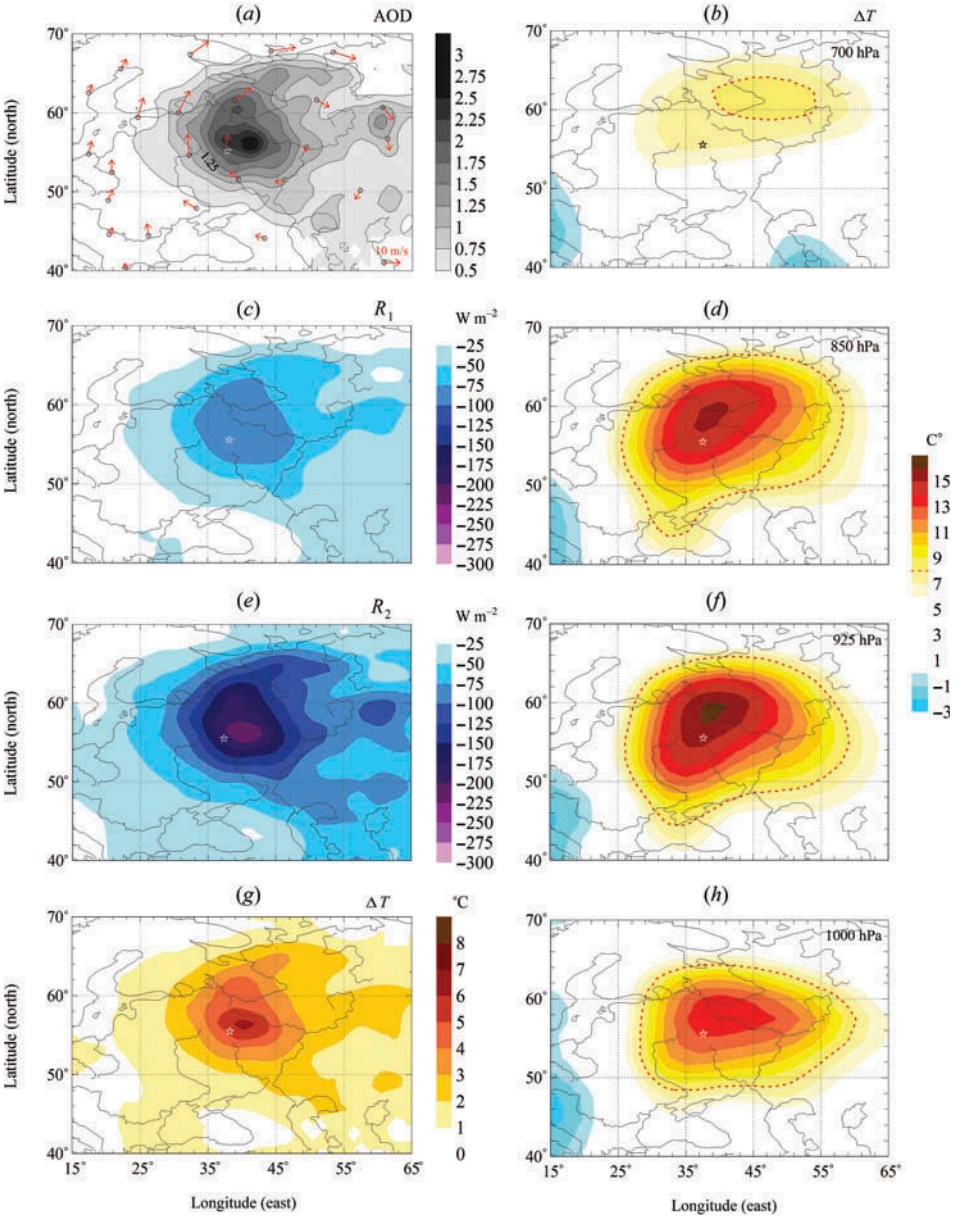

Figure 3. Spatial distributions over ER during 5–9 August 2010 of AOD (*a*) (red arrows represent average 700 hPa wind vectors at 25 upper-air stations), ARF at the TOA (*c*), ARF at the BOA (*e*), the estimates of temperature changes in smoke-polluted air of 500 m thickness during the day lasting 10 hours (*g*), and temperature anomalies at the levels 700 hPa (*b*), 850 hPa (*d*), 925 hPa (*f*), and 1000 hPa (h), obtained using NCEP/NCAR reanalysis data.

winds at the centre of the blocking anticyclone and by strong winds on the periphery of it, spreading thus over the territory of ER. The vortex structure of smoke distribution is clearly seen in the distribution of AOD on 9 August (Figure 5(*e*)).

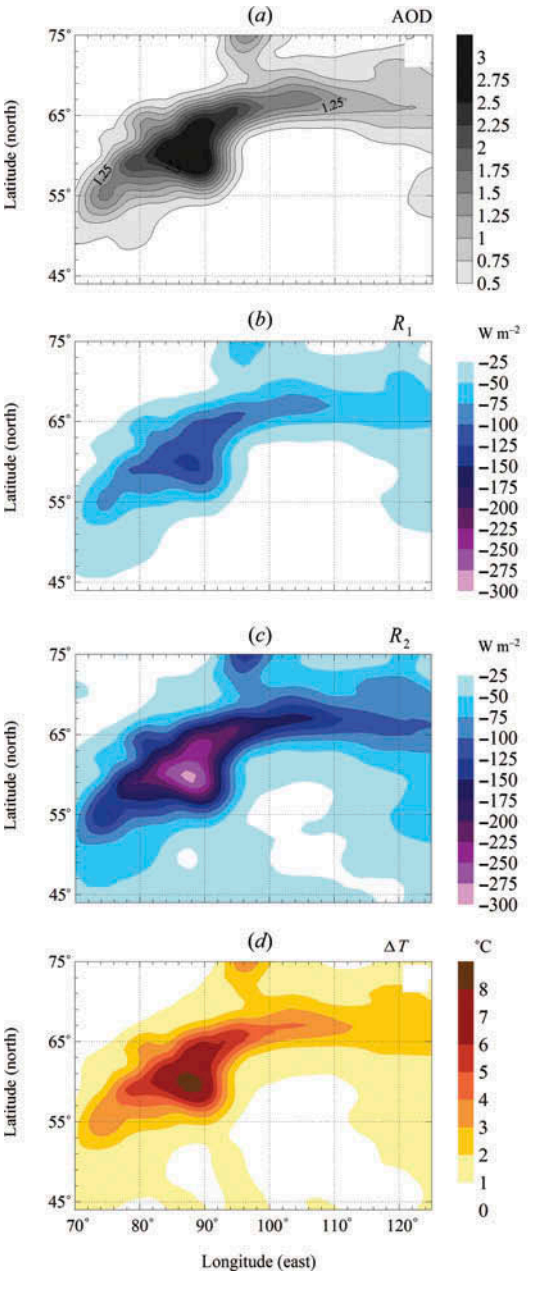

Figure 4. Spatial distributions over WS during 27–31 July 2012 of AOD (*a*), ARF at the TOA (*b*), ARF at the BOA (*c*), and the estimates of temperature changes in smoke-polluted air of 500 m thickness during the day lasting 10 hours (*d*).

Despite the ubiquity of wildfires, the daily AOD distributions over ER reveal a localized domain of high AOD values ($\tau_{0.55} > 1.5$) which was distinguished by larger integrity and connectedness in comparison with other parts of AOD distributions. It can be seen from Figure 5 that this domain and smaller inhomogeneities in AOD distributions

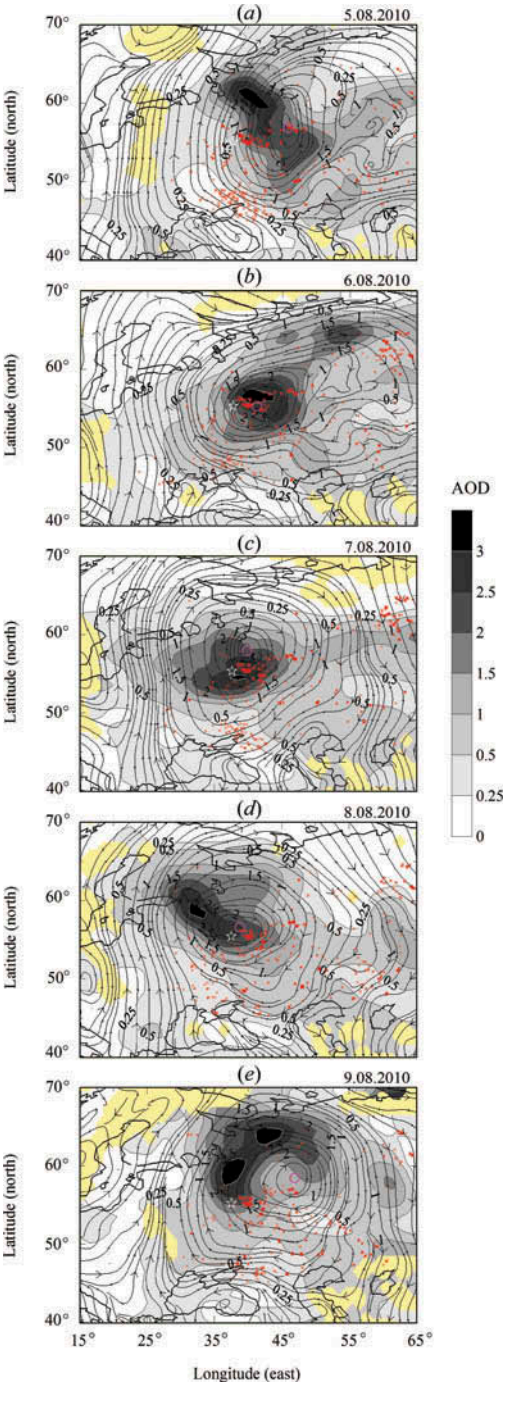

Figure 5. Daily spatial distributions of AOD over ER during 5–9 August 2010 (grey scale, yellow areas denote data absence). Red symbols denote the locations of active fires. Isolines with arrows represent the streamlines of the wind field. In each plot, an asterisk indicates the location of Moscow and a magenta circle denotes the centre of blocking anticyclone.

Table 1. Maxima of daily AODs over ER ($\tau_{0.55}^{Max}$) and their coordinates (N, E), daily AODs over Moscow ($\tau_{0.55}^{Mos}$) and Zvenigorod ($\tau_{0.55}^{Zven}$), and daily regional mean AODs over the territory of ER ($\tau_{0.55}^{ER}$) in the period 5–9 August 2010.

Date	$\tau_{0.55}^{Max}$	North	East	$\tau_{0.55}^{Mos}$	$\tau_{0.55}^{Zven}$	$\tau_{0.55}^{ER}$
5 August	4.29	61.5°	37.5°	0.63	0.42	0.98
6 August	4.80	55.5°	40.5°	1.61	1.30	1.03
7 August	4.86	53.5°	37.5°	3.14	2.82	0.99
8 August	4.17	58.5°	32.5°	2.92	3.05	1.05
9 August	4.39	59.5°	37.5°	2.61	2.37	1.16

display elements of anticyclonic circulation. Tracing in space and time the position of the extremely dense smoke domain ($\tau_{0.55} > 3$) reveals that during the period from 5 to 9 August, the region of extremely high AOD values completed a full anticyclonic rotation around Moscow, remaining at a distance of 200–650 km from the megacity.

Table 1 presents the maximum AOD values over ER (with a resolution of 1° × 1°) and their coordinates, the AODs for the pixels containing Moscow (55°–56° N, 37°–38° E) and ZSS (55°–56° N, 36°–37° E), and daily regional mean AODs during the period 5–9 August. The maximum AOD ($\tau_{0.55} = 4.86$) was observed on 7 August at 250 km south of Moscow. It follows from Table 1 that during 5–9 August the maximum daily values of AOD over ER exceeded the daily mean AOD values observed in this period over Moscow by factors of 1.5–3. The migration of the plume with extreme smoke pollution on the megacity would have caused notably more severe consequences for the health of Moscow's inhabitants than those observed. Since the anticyclone centre for a long time was located over the central cluster of wildfires, the Moscow region was predisposed to prolonged smoky conditions compared with the periphery of ER, where smoke could be rather strong, but short-lived.

Being quasi-stationary, the anticyclone experienced some changes. Analysis of the wind fields in Figure 5 shows that the migration of the anticyclone centre from east to west during 5–7 August and from west to east during 8–9 August was accompanied by appropriate migration of the areas of high AOD values. The circulation in the region occupied by the blocking anticyclone was characterized by a noticeable asymmetry. Due to a convergence of the airflows above the southwestern and western parts of the region, the speed of the wind in the rear part of the anticyclone increased from south to north. In front of the anticyclone, because of the divergence of the airflows, the flow rate decreased from north to south.

The average wind speed over the northern periphery of ER during 1–10 August 2010 reached 14 m s^{-1}, which was more than three times greater than the average wind speed over the southern periphery of ER in this period. The wind field markedly changed from day to day. On 5 and 6 August in the eastern part of ER, the atmospheric dynamics seemed rather blurred, while the days 7, 8, and 9 of August were characterized by formation of closed anticyclonic circulation over ER that led to the growth of the regional mean AOD up to its absolute maximum (1.16) on 9 August (Figure 6(*a*)).

Figure 6(*a*) shows the time series of AOD averaged over the territories of ER and WS during the periods 15 July to 20 August of both 2010 and 2012. The maximum/average values of regional mean AOD over ER and WS were close to each other, being equal to 1.16/0.53 ± 0.05 and 1.08/0.52 ± 0.05, respectively. Despite the similarity of the regional mean AOD values, the empirical probability distribution functions (EPDFs) of AODs during the periods of extreme smoke pollution over ER (5–9 August 2010) and WS

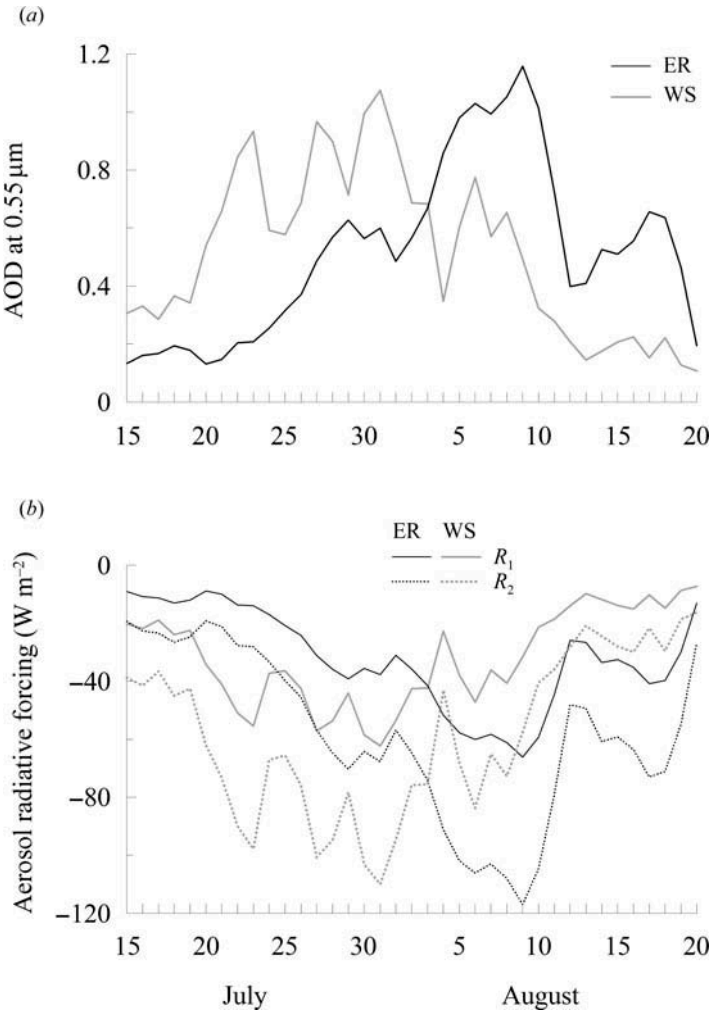

Figure 6. Temporal variations of regional mean values of AODs (*a*) and ARFs (*b*) at the TOA (R_1) and at the BOA (R_2) over ER and WS during 15 July to 20 August 2010.

(27–31 July 2012) were found to be significantly different (Figure 7). The EPDF of AOD over ER reveals unimodal distribution with a maximum in the range 0.6–0.8 characterized by essentially less half-width than that over WS. The EPDF of AOD over WS has a more complex shape. It reveals an absolute maximum at low AODs (<0.4), but also has additional peaks in the bins 1.4–1.6 and 2.4–2.6. As compared with ER, over WS the small AODs (<0.4) and high AODs (>2.2) were more frequently observed, but AODs in the range 0.8–1.8 were less frequently observed.

4.2.2. Radiative effects of smoke events

The presence of smoke in the air changes the radiation and heat balance of the atmosphere and underlying surface (Tzanis and Varotsos 2008). To meet the challenges of climate

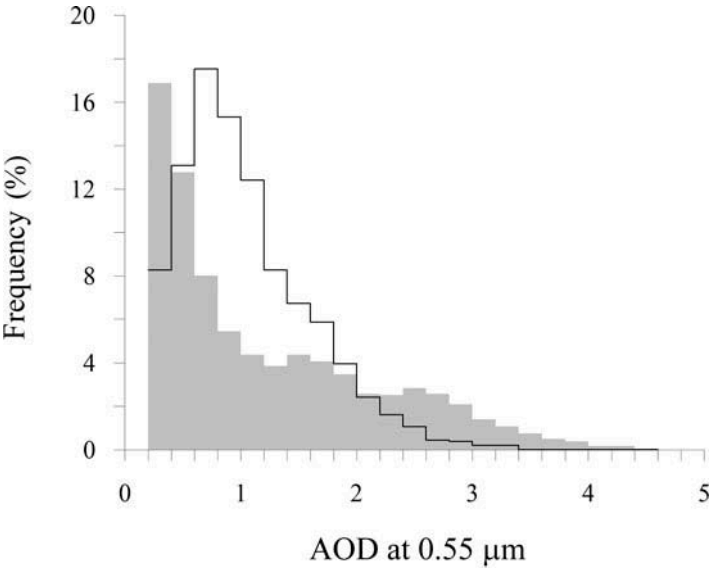

Figure 7. Empirical probability distribution functions of AOD observed during 5–9 August 2010 over ER (step line) and during 27–31 July 2012 over WS (shaded area). The EPDFs are smoothed by 3-gradation moving average.

theory, the regional mean and spatially distributed radiative effects of smoke are even more important than its local radiative effects.

An impact of aerosols on the radiative regime of the atmosphere (Varotsos et al. 2006) is evaluated by the value of the aerosol radiative forcing (ARF) effects at the top (R_1) and at the bottom (R_2) of the atmosphere. ARF effects depend on the solar zenith angle, aerosol optical characteristics, water vapour absorption, and surface reflectance. The effects are a measure of the change in the net radiation in the presence of aerosol particles in the air and in their absence. The net radiation is defined as the difference between incoming (to the layer) and outgoing (from the layer) radiation. Because of the relatively weak effect of smoke aerosols on longwave radiation, only estimates of shortwave ARF effects will be considered below.

Calculations of ARF effects are based on solving the radiative transfer equation in a plane-parallel atmosphere, taking into account scattering and absorption of solar radiation by aerosol, molecular scattering, and absorption of radiation by atmospheric gases, including H_2O, CO_2, O_2, and O_3. Optical characteristics of aerosol in the atmosphere are determined by spectral-dependent AOD, SSA, and the phase function. According to the photometric observations in the smoky atmosphere of Moscow and Moscow region in the summer of 2010, the average values of SSA and asymmetry parameter at the wavelength of 0.675 μm were equal to 0.95 and 0.63, respectively (Chubarova et al. 2011, 2012).

It should be noted that, due to weak cloudiness during the mass fires in 2010, the indirect radiative effects of smoke were insignificant as compared with the direct radiative effects of smoke. Gorchakov, Sviridenkov, et al. (2011) showed that the AOD changes during wildfires 2010 in ER were mainly conditioned by variations in concentration of smoke particles in the air.

Satellite estimates of R_1 and R_2 in this paper are based on AERONET radiation products, which include the calculations of ARF effects. Chubarova et al. (2012) presented calculations of R_1 in Moscow for AODs observed during the summer wildfires in 2002 and 2010 and for AODs observed in the years without wildfires (2001, 2003–2009). The dependence of R_1 on AOD presented in that study can rather accurately be approximated by the function of the form

$$R_1 = -0.748\,\tau_{0.50}^3 + 11.54\,\tau_{0.50}^2 - 69.47\,\tau_{0.50}. \quad (1)$$

The errors of approximation (1) are determined mainly by scattering of R_1 data at a fixed AOD and do not exceed ±15 W m^{-2}. According to the results of Gorchakova and Mokhov (2012), in a cloudless atmosphere, R_2 can be approximated as

$$R_2 = -R_0\,\tau_{0.55}^{0.83}, \quad (2)$$

where $\ln R_0 = 4.64$. Application of approximations (1) and (2) to the satellite AOD data allows us to reconstruct the distribution of smoke radiative effects over the territory of ER during the summer 2010 wildfires.

Figure 3(*a*) shows the spatial distribution of mean AOD values during the period 5–9 August 2010. The average wind vectors, calculated for the first ten days of August 2010 at 700 hPa pressure level over 25 upper-air stations (see also Sitnov and Mokhov 2013), are also depicted. It is seen from the figure that the highest AOD values were located near the centre of anticyclonic rotation (at 700 hPa level).

Figures 3(*c*) and (*e*) show the spatial distributions of corresponding mean R_1 and R_2 values in this period. The difference R_1–R_2 characterizes the intensity of heating of the smoke atmosphere. As follows from comparison of Figure 3(*c*) with Figure 3(*e*), both R_2 and R_1 were negative, but R_2 significantly exceeded R_1 (by absolute value). Thus, in the shortwave range of the solar spectrum, an abundance of smoke in the atmosphere resulted in cooling of the Earth's surface (and the air adjacent to the surface) and heating of the atmospheric column. Distributions of R_1 and R_2 are qualitatively similar to the corresponding distributions of AOD and characterized by high spatial inhomogeneities. Calculations show that on 7 August, the local latitudinal gradients of R_1 (R_1–R_2) in the north and south ER reached 39 and −50 (−30 and 50) W m^{-2} 100 km^{-1}, respectively. On 9 August, the local zonal gradients of R_1 and R_1–R_2 achieved values of −108 and 127 W m^{-2} 100 km^{-1}, respectively.

Temporal evolution of daily regional mean values of R_1 and R_2 over ER during the period from 15 July till 20 August 2010 is shown in Figure 6(*b*). During the whole period of extreme smoke loading (5–9 August 2010), the regional mean R_1 and R_2 were an average of −61 (±1) W m^{-2} and −107 (±2) W m^{-2} respectively, and on 9 August 2010 they reached values of −66 (±2) W m^{-2} and −117 (±3) W m^{-2} (standard deviations of the mean values are represented in parenthesis). The maximum local (1° × 1°) values of R_1 and R_2 in this period were equal to −128 and −269 W m^{-2}.

The similarity of optical and microphysical characteristics of smoke over ER in 2010 and over WS in 2012 allows estimation of the aerosol radiative effects over WS using approximations (1) and (2). Figures 4(*b*) and (*c*) show the spatial distributions of the mean radiative effects of smoke aerosol at the top of the atmosphere (TOA) and at the bottom of the atmosphere (BOA) during the period of maximum smoke pollution over WS. Temporal evolution of the regional mean values of R_1 and R_2 during the period 15 July to 20 August 2012 over WS is presented in Figure 6(*b*). It is seen that on 31 August 2012,

the values R_1 and R_2 peaked at −61 (±2) W m^{-2} and −110 (±3) W m^{-2}, respectively. During the period of extreme smoke loading (27–31 July 2012), the regional mean values of R_1 and R_2 over WS were equal to −54 (±2) W m^{-2} and −96 (±3) W m^{-2}, while the local (1° × 1°) R_1 and R_2 in this period reached −146 and −356 W m^{-2}. Thus, the regional mean ARF effects over ER were higher than the regional mean ARF effects over WS. On the contrary, the local ARF effects over WS were higher than those over ER. It is worth noting that Aher et al. (2014) obtained ARF values over an urban tropical observing site, Pune (India), in the range −58.16 ± 2.7 W m^{-2} to −70.56 ± 2.75 W m^{-2}, and over a coastal Arabian Sea site, Alibaug (India), in the range −78.26 ± 3.56 W m^{-2} to −83.05 ± 3.85 W m^{-2}, during the intense dust storm event of March 2012. These ARF values are considerably smaller than the regional mean ARF values over ER and WS.

4.2.3. *Thermal effects of smoke events*

Positive differences of ARF at the TOA and at the BOA are evidence for heating of the smoke layer by shortwave solar radiation. Additional heat in the smoky atmospheric column with the cross-sectional area S during time Δt is equal to

$$\Delta Q = (R_1 - R_2) S \Delta t. \tag{3}$$

Almost all of this heat is spent for heating of ambient air of volume $V = SH$, where H is the thickness of the smoke layer. Acquired heat is associated with changes in temperature by the relationship

$$\Delta Q = \rho_a C_p V \Delta T, \tag{4}$$

where ρ_a is the mass density of air (average values for ER and Siberia are 1.15 and 1.18 kg m^{-3}, respectively), C_p is the heat capacity at constant pressure (1005 J kg K^{-1}), and ΔT is the increase in air temperature during time Δt. Equating the right-hand parts of (3) and (4), one can obtain the relationship for estimating the thermal effects of smoke:

$$\frac{\Delta T}{\Delta t} = \frac{R_1 - R_2}{\rho_a C_p H}. \tag{5}$$

Regional mean values of AOD over ER during the period 5–9 August 2010 varied between 0.98 and 1.16. When $\tau_{0.55} = 1$, the difference R_1–R_2 is equal to 45 W m^{-2}, and the rate of temperature increase due to absorption of the shortwave solar radiation in the smoky layer of 500 m (1000 m) thickness is about 0.26 (0.13)°C hour^{-1}. Maximum values of $\tau_{0.55}$ during the period of extreme smoke (with a resolution of 1° × 1°) exceeded 4. The rate of temperature increase in such conditions exceeds 1.0°C hour^{-1}.

Figure 3(*g*) shows the estimates of temperature changes in the 500 m smoky layer for a 10-hour period that corresponds to the distribution of R_1–R_2. It can be seen that the thermal effects of smoke, reflecting the distribution of AOD, are characterized by a substantial spatial heterogeneity. The maximum heating rate (more than 0.6°C hour^{-1}) was observed in the central part of ER, whereas over the periphery of ER the magnitudes of temperature effects were reduced by 3–4 times. Spatial inhomogeneity of the thermal effects could lead to the formation of appropriate spatial temperature inhomogeneities. Strengthening the horizontal gradients of temperature should increase atmospheric

Table 2. Values above the line represent the area (in million km^2) occupied by temperature anomalies (Δt) at different pressure levels in the period 5–9 August 2010; values below the line represent the same, but expressed as a percentage of the territory, restricted by coordinates 40 N–70 N, 15 E–65 E, with an area of 10,850,031 km^2.

	500 hPa	700 hPa	850 hPa	925 hPa	1000 hPa
$\Delta t > 5°$	1.43	3.73	6.34	6.04	5.13
	13	34	58	56	47
$\Delta t > 7.5°$	–	1.02	3.94	3.85	3.07
		9	36	35	28
$\Delta t > 10°$	–	–	2.24	2.39	1.73
			21	22	16
$\Delta t > 12.5°$	–	–	1.07	1.28	0.56
			10	12	5
$\Delta t > 15°$	–	–	0.08	0.35	–
			1	3	

instability, inducing thus the air motions, in particular, arising of thermal wind. It should also be noted that the heating of smoke, concentrated in the centre of the anticyclone, should strengthen the blocking anticyclone, and thus prolong its existence.

Figures 3(*b*), (*d*), (*f*), and (*h*) show the temperature anomalies at the pressure levels 700, 850, 925, and 1000 hPa obtained using NCEP/NCAR reanalysis data. These anomalies were calculated as deviations of local temperatures averaged over the period 5–9 August 2010 from the corresponding local temperatures averaged over the periods 5–9 August 2000–2009. It can be seen that the spatial distributions of the anomalies display the maximum centred near the maximum of the AOD, R_1, R_2, and $\Delta T/\Delta t$. The temperature anomalies reach their absolute maximum (16.2°C) at the level of 925 hPa (~800 m), while at the levels of 1000, 850, and 700 hPa the maximum values of the anomalies did not exceed 13.8°C, 15.2°C, and 8.6°C, respectively.

Table 2 presents the sizes of areas covered by the temperature anomalies whose magnitudes in early August 2010 exceeded 5°C, 7.5°C, 10°C, 12.5°C, and 15°C at the levels of 500, 700, 850, 925, and 1000 hPa, respectively. It can be seen that anomalies of temperature exceeding 5°C were observed in this period up to the 500 hPa level (and even higher), and that the anomalies of the same magnitude embraced the maximum areas not in the surface layer (at 1000 hPa), but rather at altitudes between the 925 and 850 hPa levels, that is, the maximum heating of smoky air was observed at altitudes of about 1 km. However, a comparison of Figures 3(*f*) and (*g*) shows that the existing temperature anomalies were significantly greater than temperature anomalies, which could be explained solely by radiative heating of smoky air. It is known that the region of anticyclonic circulation is characterized, on the whole, by the downward movement of air, and thus additional heating could be due to an adiabatic warming of the descending air. Some contribution to the formation of the temperature profile over ER could make the advection of hot dry air from Central Asia and warm humid air from the North Atlantic and Mediterranean Sea (Sitnov and Mokhov 2013). It should also be noted that the local thermal regime in Moscow in the summer of 2010 was subjected to an urban heat island (Gorchakov et al. 2013).

The regional mean AOD over WS during the period 27–31 July 2012 was equal to 1.0, which is quite close to that over ER during the period 5–9 August 2010. The rate of temperature increase due to absorption of shortwave solar radiation in the smoky layer of

500 m thickness corresponding to AOD = 1.0, as stated earlier, is about 0.26°C hour^{-1}. Maximum local values of AOD during the period of extreme smoke reached a value of 4.43 in the ground pixel 88°–89° N, 60°–61° E. The rate of the temperature increase in such conditions was equal to 1.2°C hour^{-1}.

Summarizing the comparison, it should be noted that when considering the 5-day period of maximum smoke pollution and the equal territories centred on most intensive clusters of fires, the overall number of active fires and also the regional mean AOD values, as well as the radiative and thermal effects of smoke aerosol during the wildfires in the summer 2010 over ER and those in the summer 2012 over WS, were found to be approximately equal. At the same time the local AOD values and modulo R_1 and R_2 over WS were significantly higher than those over ER. This fact is indicative of greater heterogeneity of smoke pollution of the territory of WS in 2012 as compared with the territory of ER in 2010. Localization of high values of AOD in the centre ER was due to the predominance in the region of closed anticyclonic circulation due to omega blocking, which favoured the smoke aerosols to stay longer in the region. Over WS, the aerosols formed during the wildfires were more effectively removed from the considered domain by prevailing southwest winds.

4.3. *Analysis of ground-based observations*

4.3.1. *Optical and microphysical properties of smoke aerosol*

Optical characteristics of smoke aerosols in the summer of 2010 over ER were quite distinct from those for typical atmospheric aerosol (Eck et al. 1999). Thus, the spectral dependence of AOD obtained at ZSS on 8 August 2010 with a satisfactory accuracy could be approximated in log-log scale by a convex parabola (Figure 8). The AOD values averaged over 1–10 August 2010 revealed the same peculiarity (Gorchakov, Sviridenkov, et al. 2011). An analysis of the spectral behaviour of AOD in smoky conditions over WS

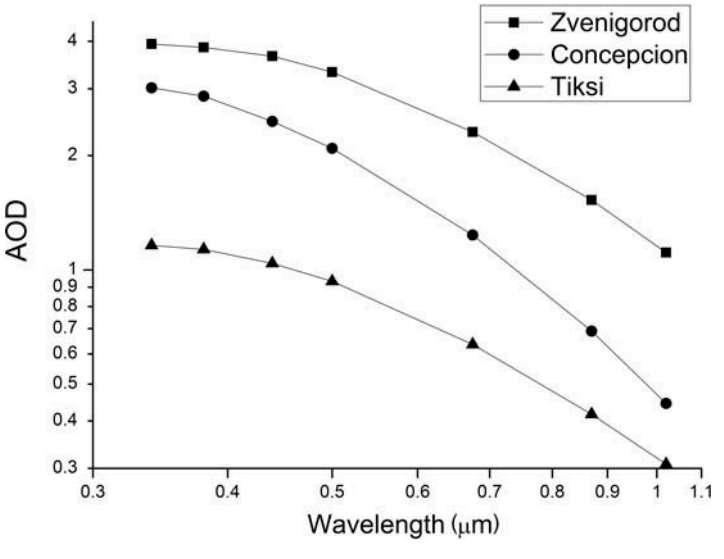

Figure 8. Spectral dependence of AOD in the smoky atmosphere over AERONET stations Zvenigorod (8 August 2010), Concepcion, Bolivia (24 August 1998), and Tiksi (26 July 2012).

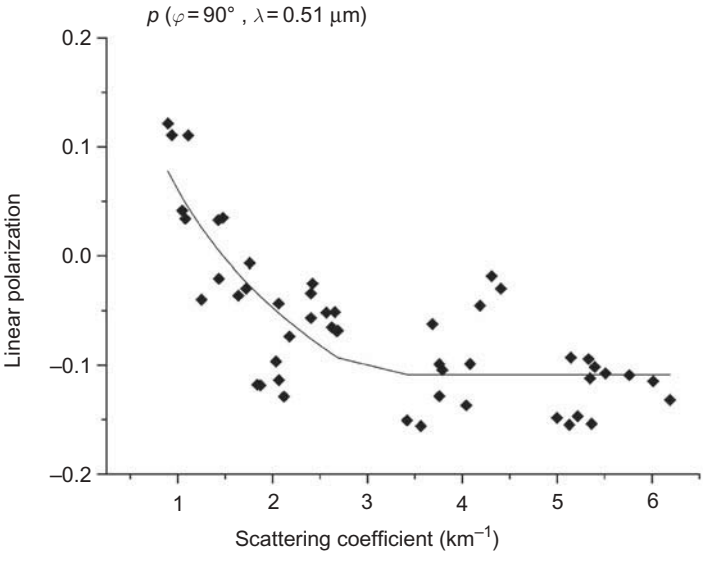

Figure 9. Correlation between the degree of linear polarization (p) and scattering coefficient in the surface layer in the Moscow region (August 2010).

in the summer of 2012 showed that $\tau(\lambda)$ at the AERONET station Tiksi could be also approximated by a convex parabola (Figure 8). The above-mentioned peculiarity of spectral dependency of AOD was found not only in the smoky conditions over ER in the summer of 2010 and over WS in the summer of 2012, but also during wildfires of 1998 in Bolivia. As an example, the spectral dependence of AOD obtained at the AERONET station, Concepcion, on 24 August 1998 is also shown in Figure 8. Spectral dependences of AODs at considered AERONET stations can be expressed as $\ln(\tau) = -0.96(\ln\lambda)^2 - 2.18\ln\lambda + 0.14$ (Zvenigorod), $\ln(\tau) = -1.09(\ln\lambda)^2 - 2.90\ln\lambda - 0.75$ (Concepcion), and $\ln(\tau) = -0.85(\ln\lambda)^2 - 2.13\ln\lambda - 1.15 \times$ (Tiksi).

An analysis of spectropolarimetric measurements in the atmospheric surface layer, carried out in the summer of 2010 at ZSS, showed that the degree of linear polarization (p) of light at the wavelength $\lambda = 0.51$ μm scattered at an angle $\varphi = 90°$ in conditions of dense smoke decreased to −0.1 and even to −0.15. As is known from the Mie theory, p (at $\varphi = 90°$) varies widely with r, with λ, and with a complex refractive index (n). According to AERONET data, the value of p in the smoky conditions over ER in the summer of 2010 was negative for $r = 0.2$–0.3 μm, $\lambda = 0.51$ μm, and $n = 1.5$. In the case of narrow particle size distribution, when integrating over the radius, one can expect that p still remains negative. The statistical relationship between p and the scattering coefficient σ is presented in Figure 9. It is of interest that negative values of p were observed predominantly for $\sigma > 2.0$ km^{-1}. A decrease in the degree of linear polarization of scattered light down to the value −0.1 was also found by Kozlov et al. (2013) in smoky conditions over WS in the summer of 2012.

Gorchakov, Sviridenkov, et al. (2011) retrieved the volume distribution function (VDF) of smoke aerosol for the summer 2010 episode using spectropolarimetric and sun-sky photometer data (Dubovik and King 2000) at ZSS and inferred that non-typical optical properties of smoke over ER in the summer of 2010 were conditioned by a narrow VDF with an effective radius of 0.2–0.3 μm. They found that the VDF of the fine aerosol

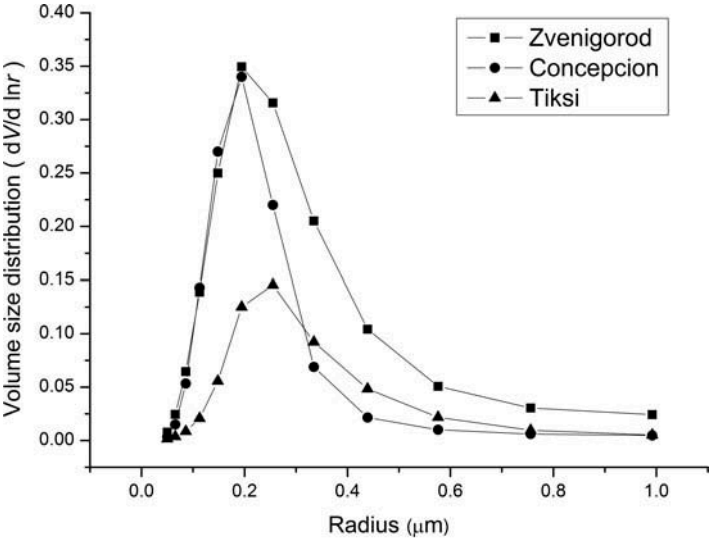

Figure 10. Aerosol particle volume size distributions in the smoky atmosphere over AERONET stations Zvenigorod (9 August 2010), Concepcion, Bolivia (24 August 1998), and Tiksi (26 July 2012).

fraction in the atmospheric column at high AOD and in the surface layer at high σ could be approximated by lognormal distribution:

$$\frac{dV}{d\ln r} = \frac{V_0}{v\sqrt{2\pi}} \exp\left\{ -\frac{\ln^2(r/r_0)}{2v^2} \right\}, \tag{6}$$

where V_0 is the total volume of particles, r is the radius, r_0 is the median radius, and v is the standard deviation of the natural logarithm of the radius. The value v was found to be equal to 0.29. This lognormal distribution is a good approximation for the VDF of smoke aerosol for radii from 0.05 to 0.4 μm. The VDFs of aerosol at the AERONET stations Tiksi and Concepcion (Eck et al. 1999) retrieved from observations during wildfires are similar in shape to the distributions retrieved at ZSS in summer of 2010 (Figure 10). In all considered cases, the submicron mode was responsible for major contribution to the aerosol extinction.

According to AERONET retrievals, the SSA of smoke aerosol over ER in the summer of 2010 was very high (0.95 at $\lambda = 0.44$ μm and 0.975 at $\lambda = 0.87$ μm). Similar estimates of the SSA of smoke aerosol in the visible spectral range (0.95–0.98) in the atmospheric surface layer during the wildfires of 2012 in WS were obtained by Kozlov et al. (2013). Agreement should be noted between the optical and microphysical aerosol characteristics during wildfires over ER in 2010 and over WS in 2012.

4.3.2. *Air pollution in smoky atmosphere*

Surface pollution in the Moscow region during the period of intense forest and peat bog fires in ER in summer 2010 was studied using data obtained at automatic control stations of the Mosecomonitoring State Environmental Protection Enterprise (Gorchakov, Sviridenkov, et al. 2011; Golitsyn et al. 2011). Analysis showed that during the period

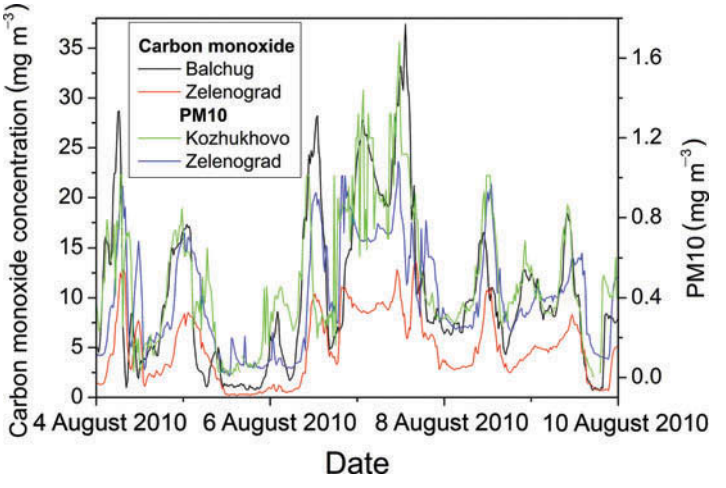

Figure 11. Aerosol mass concentration (PM10) and carbon monoxide concentration in the smoky atmosphere of the Moscow region during the period 4–10 August 2010.

from 4 August to 10 August 2010 the mass concentration of aerosol (PM10) and soot concentration at several stations, including Kozhukhovo, reached the values 1.7 mg m^{-3} and 22 μg m^{-3}, respectively (Figure 11). It is worth noting that according to the results of Kozlov et al. (2013), the PM10 in Tomsk during the wildfires in the summer of 2012 in WS reached 1.5 mg m^{-3}.

The highest surface CO concentrations in Moscow reached 37.5 mg m^{-3} and were observed in Moscow's downtown (Balchug station). The total CO content over the Moscow region according to the spectroscopic observations reached 6 g m^{-2} or 12.7×10^{18} mol cm^{-2} (Golitsyn et al. 2011). Time series of the CO concentrations at the stations Balchug (Moscow's downtown) and Zelenograd (Moscow's suburb) demonstrate a high variability of CO in the Moscow region. The correlation analysis of CO and PM10 showed that in the smoky conditions and when the CO concentrations exceed 6–7 mg m^{-3}, the value of PM10 can be estimated using the approximate ratio PM10 = 0.08 × [CO]. Thus, the maximum PM10 value in the smoky atmosphere of Moscow megacity can reach values of about 3.5 mg m^{-3}. The geometrical thickness of the smoke layer was estimated using the CO measurements at the Ostankino TV tower (of 540 m height) located in the north of Moscow. Figure 12 shows the typical vertical profiles of CO concentrations during the period from 4 August to 9 August 2010. The thickness of the smoke layer in the urban atmosphere as a rule did not exceed 500 m.

5. Conclusion

An analysis of two large-scale smoke events, caused by the wildfires in ER in the summer of 2010 and in WS in the summer of 2012, conducted over the equal territories 47°–65° N, 25°–55° E, and 51°–70° N, 71°–104° E (of approximately 4×10^6 km^2 each), and over the equal time intervals 5–9 August 2010 and 27–31 July 2012 (which are the periods of maximum regional smoke pollution) was carried out. The results showed that the overall number of fires in ER (4754) exceeded that in WS (3823); nevertheless, the regional mean AODs over ER and WS were found to be practically equal (1.02 ± 0.02 and 1.00 ± 0.04).

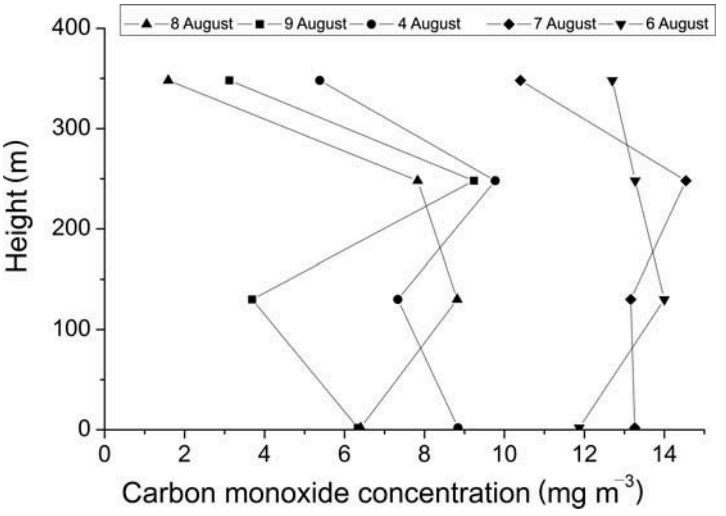

Figure 12. Carbon monoxide concentration profiles (Moscow, Ostankino) in the smoky atmosphere: 4 August (04:00–09:00 (local time)), 6 August (11:00–15:40), 7 August (11:20–20:00), 8 August (09:00–15:20), and 9 August (10:40–13:40).

The regional mean radiative forcing effects at the TOA (BOA) over ER and WS were also found to be close to each other: -61 ± 1 (-107 ± 2) W m^{-2} and -54 ± 2 (-96 ± 3) W m^{-2}, respectively. Based on these estimates, the regional mean radiative heating rate of the atmosphere for both events was evaluated to be 0.26°C hour^{-1}. With this, the radiative heating was characterized by strong spatial inhomogeneity. It was maximum in the central parts of the considered territories, reaching the values 1–1.2°C hour^{-1}, while at the peripheries of ER and WS it was diminished almost by an order. A comparison of estimated thermal effects of smoke with temperature anomalies, calculated using NCAR/NCEP reanalysis data, showed that temperature anomalies observed over ER during the wildfires of the summer 2010 were significantly higher (up to 16.2°C at 925 hPa) than the changes of temperature, which could be caused solely by radiative heating of smoky air. Additional heating could be apparently conditioned by adiabatic processes due to descending motions, which are characteristic for anticyclone conditions.

Optical and microphysical properties of aerosols during the wildfires in ER in 2010 and in WS in 2012 also revealed some similar characteristics. Thus, smoke aerosols were found to be predominantly in the submicron fraction and characterized by very high SSA values (0.95–0.98). The spectral dependence of AODs in log-log scale could be approximated by a convex parabola. In cases of dense smoke (at $\sigma > 2$ km^{-1}), the degree of linear polarization at the scattering angle 90° during both events decreased to negative values and ranged between −0.1 and −0.15. Abnormal optical properties of aerosols in the surface layer and atmospheric column during the wildfires were mainly due to unusually narrow particle size distribution.

Along with the similarities, there were differences between the considered smoke events. Thus, the local (1° × 1°) 5-day average values of AOD in WS reached 4.43, which significantly exceeded the local 5-day average values of AOD in ER (3.16). The differences between the regimes of smoke pollution in ER and WS revealed themselves in the differences between EPDFs of AOD. The EPDF of AOD over ER revealed unimodal distribution with a maximum in the range 0.6–0.8 and characterized by essentially less

half-width than that over WS, which has a more complex shape and revealed a hint on polymodal distribution with the main maximum at AODs less than 0.4 and additional peaks in the ranges 1.4–1.6 and 2.4–2.6. The differences in the regimes of smoke pollution were apparently due to the differences in the transport of smoke by wind, conditioned by regional atmospheric circulation, associated in turn with the different types of atmospheric blocking occurring over ER and WS during the periods under review.

A comparison between MODIS AOD (L3) data obtained over the ground pixel 55°–56° N, 36°–37° E with AOD data obtained by the sun-sky photometer CIMEL at the AERONET station Zvenigorod (55.7° N, 36.8° E) during the 2010 wildfires revealed satisfactory agreement.

Acknowledgements

We acknowledge the MODIS mission scientists and associated NASA personnel for production and free access to aerosol and active fire data used in this research. We are also indebted to NASA for AERONET data and the Mosecomonitoring State Environmental Protection Enterprise for the ecological monitoring data. We are grateful to Prof. Yu.M. Timofeev for helpful discussion and two anonymous reviewers for criticism and valuable comments.

Funding

This work was supported by the Russian Foundation for Basic Research grants: [12-05-91057-CNRS, 13-05-00956, 13-05-41432, and 14-05-00639].

References

Acker, J. C., and G. Leptoukh. 2007. "Online Analysis Enhances Use of NASA Earth Science Data." *Eos, Transactions, American Geophysical Union* 88: 14–17. doi:10.1029/2007EO020003.

Aher, G. R., G. V. Pawar, P. Gupta, and P. C. S. Devara. 2014. "Effect of Major Dust Storm on Optical, Physical, and Radiative Properties of Aerosols over Coastal and Urban Environments in Western India." *International Journal of Remote Sensing* 35: 871–903. doi:10.1080/01431161.2013.873153.

Chubarova, N., E. Nezval', M. Sviridenkov, A. Smirnov, and I. Slutsker. 2012. "Smoke Aerosol and its Radiative Effects During Extreme Fire Event over Central Russia in Summer 2010." *Atmospheric Measurement Techniques* 5: 557–568. doi:10.5194/amt-5-557-2012.

Chubarova, N. E., E. V. Gorbarenko, E. I. Nezval', and O. A. Shilovtseva. 2011. "Aerosol and Radiation Characteristics of the Atmosphere during Forest and Peat Fires in 1972, 2002, and 2010 in the Region of Moscow." *Izvestiya, Atmospheric and Oceanic Physics* 47: 729–738. doi:10.1134/S0001433811060028.

Davies, D. K., S. Ilavajhala, M. M. Wong, and C. O. Justice. 2009. "Fire Information for Resource Management System: Archiving and Distributing MODIS Active Fire Data." *IEEE Transactions on Geoscience and Remote Sensing* 47: 72–79. doi:10.1109/TGRS.2008.2002076.

Dubovik, O., and M. D. King. 2000. "A Flexible Inversion Algorithm for Retrieval of Aerosol Optical Properties from Sun and Sky Radiance Measurements." *Journal of Geophysical Research* 105: 20673–20696. doi:10.1029/2000JD900282.

Eck, T. F., B. N. Holben, J. S. Reid, O. Dubovik, A. Smirnov, N. T. O'Neill, I. Slutsker, and S. Kinne. 1999. "Wavelength Dependence of the Optical Depth of Biomass Burning, Urban, and Desert Dust Aerosols." *Journal of Geophysical Research* 104: 31333–31349. doi:10.1029/1999JD900923.

Giglio, L., J. Descloitres, C. O. Justice, and Y. J. Kaufman. 2003. "An Enhanced Contextual Fire Detection Algorithm for MODIS." *Remote Sensing of Environment* 87: 273–282. doi:10.1016/S0034-4257(03)00184-6.

Golitsyn, G. S., G. I. Gorchakov, E. I. Grechko, E. G. Semoutnikova, V. S. Rakitin, E. V. Fokeeva, A. V. Karpov, G. A. Kurbatov, E. S. Baikova, and T. P. Safrygina. 2011. "Extreme Carbon Monoxide Pollution of the Atmospheric Boundary Layer in Moscow Region in the Summer 2010." *Doklady Earth Sciencies* 441: 1666–1672.

Gorchakov, G., E. Semoutnikova, A. Karpov, and E. Lezina. 2011. "Air Pollution in Moscow Megacity." In *Advanced Topics in Environmental Health and Air Pollution Case Studies*, edited by A. M. Moldoveanu, 211–236. Rijeka: InTech.

Gorchakov, G. I., P. P. Anikin, A. A. Volokh, A. S. Emilenko, A. A. Isakov, V. M. Kopeikin, T. Y. Ponomareva, E. G. Semutnikova, M. A. Sviridenkov, and K. A. Shukurov. 2004. "Studies of the Smoky Atmosphere Composition over Moscow During Peatbog Fires in the Summer-Fall Season of 2002." *Izvestiya, Atmospheric and Oceanic Physics* 40: 323–336.

Gorchakov, G. I., E. N. Kadygrov, V. E. Kunitsyn, V. I. Zakharov, E. G. Semoutnikova, A. V. Karpov, G. A. Kurbatov, E. A. Miller, and S. I. Sitansky. 2013. "Moscow Heat Island and Thermal Anomaly into Blocking Anticyclone in Summer 2010." In *Proceedings International Symposium "Atmospheric Radiation and Dynamics" (ISARD–2013)*, Petrodvorets, June 24–27, 50–51. Saint Petersburg: Saint Petersburg State University.

Gorchakov, G. I., M. A. Sviridenkov, E. G. Semoutnikova, N. E. Chubarova, B. N. Holben, A. V. Smirnov, A. S. Emilenko, A. A. Isakov, V. M. Kopeikin, A. V. Karpov, E. A. Lezina, and O. S. Zadorozhnaya. 2011. "Optical and Microphysical Parameters of the Aerosol in the Smoky Atmosphere of the Moscow Region in 2010." *Doklady Earth Sciences* 437: 513–517. doi:10.1134/S1028334X11040131.

Gorchakova, I. A., and I. I. Mokhov. 2012. "The Radiative and Thermal Effects of Smoke Aerosol over the Region of Moscow during the Summer Fires of 2010." *Izvestiya, Atmospheric and Oceanic Physics* 48: 496–503. doi:10.1134/S0001433812050039.

Holben, B. N., T. F. Eck, I. Slutsker, D. Tanre, J. P. Buis, A. Setzer, E. Vermote, J. A. Reagan, Y. J. Kaufman, T. Nakajima, F. Lavenu, I. Jankowiak, and A. Smirnov. 1998. "AERONET – A Federated Instrument Network and Data Archive for Aerosol Characterization." *Remote Sensing of Environment* 66: 1–16. doi:10.1016/S0034-4257(98)00031-5.

Huang, F., X. Tang, S. Y. Lou, and C.-H. Lu. 2007. "Evolution of Dipole-Type Blocking Life Cycles: Analytical Diagnoses and Observations." *Journal of the Atmospheric Sciences* 64: 52–73. doi:10.1175/JAS3819.1.

Hubanks, P. A., M. D. King, S. Platnick, and R. Pincus. 2008. "MODIS Atmosphere L3 Gridded Product." Algorithm Theoretical Basis Document No. ATBD-MOD-30.

Ichoku, C., D. A. Chu, S. Mattoo, Y. J. Kaufman, L. A. Remer, D. Tanré, I. Slutsker, and B. N. Holben. 2002. "A Spatio-Temporal Approach for Global Validation and Analysis of MODIS Aerosol Products." *Geophysical Research Letters* 29 (12): 8006. doi:10.1029/2001GL013206.

Justice, C. O., L. Giglio, S. Korontzi, J. Owens, J. T. Morrisette, D. Roy, J. Descloitres, S. Alleaume, F. Petitcolin, and Y. Kaufman. 2002. "The MODIS Fire Products." *Remote Sensing of Environment* 83: 244–262. doi:10.1016/S0034-4257(02)00076-7.

Kalnay, E. T., M. Kanamitsu, R. Kistler, W. Collins, D. Deaven, L. Gandin, M. Iredell, S. Saha, G. White, J. Woollen, Y. Zhu, M. Chelliah, W. Ebisuzaki, W. Higgins, J. Janowiak, K. C. Mo, C. Ropelewski, J. Wang, A. Leetmaa, R. Reynolds, R. Jenne, and D. Joseph. 1996. "The NMC/NCAR 40-Year Reanalysis Project." *Bulletin of American Meteorological Society* 77: 437–471.

Kaufman, Y. J., D. Tanré, H. R. Remer, E. F. Vermote, A. Chu, and B. N. Holben. 1997. "Operational Remote Sensing of Tropospheric Aerosol over Land from EOS Moderate Resolution Imaging Spectroradiometer." *Journal of Geophysical Research* 102 (D14): 17051–17067. doi:10.1029/96JD03988.

Kozlov, V. S., E. P. Yausheva, S. A. Terpugova, and M. V. Panchenko. 2013. "Optical-Microphysical Properties of Smoke Haze from Siberian Forest Fires in Summer 2012." In *Proceedings International Symposium "Atmospheric Radiation and Dynamics" (ISARD–2013)*, Petrodvorets, June 24–27, 67–68. Saint Petersburg: Saint Petersburg State University.

Levy, R. C., L. A. Remer, R. G. Kleidmann, S. Mattoo, C. Ichoku, R. Kahn, and T. F. Eck. 2010. "Global Evaluation of the Collection 5 MODIS Dark-Target Aerosol Product over Land." *Atmospheric Chemistry and Physics* 10: 10399–10420. doi:10.5194/acp-10-10399-2010.

Levy, R. C., L. A. Remer, S. Mattoo, E. F. Vermote, and Y. J. Kaufman. 2007. "Second-Generation Operational Algorithm: Retrieval of Aerosol Properties over Land from Inversion of Moderate Resolution Imaging Spectroradiometer Spectral Reflectance." *Journal of Geophysical Research* 112: D13211. doi:10.1029/2006JD007811.

Mokhov, I. I. 2011. "Specific Features of the 2010 Summer Heat Formation in the European Territory of Russia in the Context of General Climate Changes and Climate Anomalies." *Izvestiya, Atmospheric and Oceanic Physics* 47: 653–660.

Mokhov, I. I., A. V. Chernokulsky, and I. V. Shkolnik. 2006. "Regional Model Assessments of Fire Risks Under Global Climate Changes." *Doklady Earth Sciences* 411: 1485–1488. doi:10.1134/S1028334X06090340.

More, S., P. Pradeep Kumar, P. Gupta, P. C. S. Devara, and G. R. Aher. 2013. "Comparison of Aerosol Products Retrieved from AERONET, MICROTOPS and MODIS over a Tropical Urban City, Pune, India." *Aerosol and Air Quality Research* 13: 107–121. doi:10.4209/aaqr.2012.04.0102.

Sakerin, S. M., T. V. Bedareva, T. B. Zhuravleva, D. M. Kabanov, I. M. Nasrtdinov, and Y. S. Turchinovich. 2013. "Aerosol Radiative Characteristics During Smoke Mist in Siberia." In *Proceedings International Symposium "Atmospheric Radiation and Dynamics" (ISARD–2013)*, Petrodvorets, June 24–27, 67. Saint Petersburg: Saint Petersburg State University.

Salomonson, V. V., W. L. Barnes, P. W. Maymon, H. E. Montgomery, and H. Ostrow. 1989. "MODIS: Advanced Facility Instrument for Studies of the Earth as a System." *IEEE Transactions on Geoscience and Remote Sensing* 27: 145–153. doi:10.1109/36.20292.

Sitnov, S. A. 2011a. "Satellite Monitoring of Atmospheric Gaseous Species and Optical Characteristics of Atmospheric Aerosol Properties over the European Part of Russia in April–September 2010." *Doklady Earth Sciences* 437: 368–373. doi:10.1134/S1028334X11030081.

Sitnov, S. A. 2011b. "Aerosol Optical Thickness and the Total Carbon Monoxide Content over the European Russia Territory in the 2010 Summer Period of Mass Fires: Interrelation between the Variation in Pollutants and Meteorological Parameters." *Izvestiya, Atmospheric and Oceanic Physics* 47: 714–728. doi:10.1134/S0001433811060156.

Sitnov, S. A., G. I. Gorchakov, M. A. Sviridenkov, I. A. Gorchakova, A. V. Karpov, and A. B. Kolesnikova. 2013. "Aerospace Monitoring of Smoke Aerosol over the European Part of Russia in the Period of Massive Forest and Peatbog Fires in July–August of 2010." *Atmospheric and Oceanic Optics* 26: 265–280. doi:10.1134/S1024856013040143.

Sitnov, S. A., and I. I. Mokhov. 2013. "Water Vapor Content in the Atmosphere over European Russia during the Summer 2010 Fires." *Izvestiya, Atmospheric and Oceanic Physics* 49: 380–394. doi:10.1134/S0001433813040099.

Sviridenkov, M. A., A. S. Emilenko, V. M. Kopeikin, and W. Gengchen. 2006. "Transformation of Optical Properties and Microstructure of Aerosol During Smog Episode in Beijing." *Atmospheric and Oceanic Optics* 19 (6): 469–472.

Tang, X. Y., J. Zhao, F. Huang, and S. Y. Lou. 2009. "Monopole Blocking Governed by a Modified KdV Type Equation." *Studies in Applied Mathematics* 122: 295–304. doi:10.1111/j.1467-9590.2009.00434.x.

Tzanis, C., and C. Varotsos. 2008. "Tropospheric Aerosol Forcing of Climate in Greece." *International Journal of Remote Sensing* 29 (9): 2507–2517. doi:10.1080/01431160701767575.

Val Martin, M., R. A. Kahn, J. A. Logan, R. Paugam, M. Wooster, and C. Ichoku. 2012. "Space-Based Observational Constraints for 1-D Fire Smoke Plume-Rise Models." *Journal of Geophysical Research: Atmospheres* 117: D22204. doi:10.1029/2012JD018370.

Van Donkelaar, A., R. V. Martin, R. C. Levy, M. A. Da Silva, M. Krzyzanowski, N. E. Chubarova, E. G. Semutnikova, and A. J. Cohen. 2011. "Satellite-Based Estimates of Ground-Level Fine Particulate Matter during Extreme Events: A Case Study of the Moscow Fires in 2010." *Atmospheric Environment* 45: 6225–6232. doi:10.1016/j.atmosenv.2011.07.068.

Varotsos, C., J. Ondov, A. P. Cracknell, and M. Efstathiou. 2006. "Long-Range Persistence in Global Aerosol Index Dynamics." *International Journal of Remote Sensing* 27 (16): 3593–3603. doi:10.1080/01431160600617236.

Witte, J. C., A. R. Douglass, A. Da Silva, O. Torres, R. Levy, and B. N. Duncan. 2011. "NASA a-Train and Terra Observations of the 2010 Russian Wildfires." *Atmospheric Chemistry and Physics* 11: 9287–9301. doi:10.5194/acp-11-9287-2011.